Energy Shifts and Intensity Ratio of X-ray Satellites

May 12, 2006

Hideyuki Tatsuno

The SDD test experimental data taken in E549 were analyzed to check the energy shifts of X-rays ionized by charged particles . The satellite X-rays due to direct multiple ionization may influence the Kα and Kβ centroid energy. But from the test experimental data cannot be concluded because of its low statistic and poor energy calibration.

1 Introduction

Systematic shifts of the centroids of Ti and Ni Kβ X-rays were found, and these shits were about -10 eV relative to their Kα1 X-rays. When Kα1 X-rays were used for the energy calibration, the absolute values were referenced from X-ray Data Booklet, 4510.84 eV for Ti and 7478.15 eV for Ni. But the absolute values of the energy of Kα1 X-rays may have shifts due to multiple ionization, radiative Auger effect or other inner-shell processes.

In this report, I checked these possibilities to get some clues for the Kβ mean shift problem by analyzing SDD test experimental data. First, the inner-shell processes are explained and the satellite peaks of them are discussed using examples from some references. Second, SDD test experimental data taken in E549 are analyzed and the energy of X-rays photo-ionized and ionized by charged particle projection are evaluated.

2 X-ray Satellites

K series satellite can originate from transitions between multiple ionized states. In most case the satellites due to direct multiple ionization are expected to appear on the short-wavelength side of the corresponding main line. For the long-wavelength satellites of K series, two processes are recognized: (i) two-electron processes, whereby the photon energy is decreased through a simultaneous excitation of an outer electron into the continuum (radiative Auger); and (iii) the influence of multiplet splittings.

2.1 Satellites from Multiplet Splitting

The multiplet structures X-ray emission line can appear as fully resolved splitting through a sufficiently strong exchange interaction between unfilled subshells and X-ray vacancies.

The X-ray non-diagram line Kβ' so-called satellite line of the Kβ1 line has following characters; 1) the Kβ' line appears on the long wavelength side of the Kβ1 line, 2) its intensity is large in comparison with other non-diagram lines, and 3) it distinctly appears only when substance is a chemical compound having a high magnetic susceptibility.

The detail of this theory and experiment are explained by Tsutsumi [1]. They observed the energy of the Kβ' and the intensity ratio of Kβ' and Kβ1 of chromium from the various chromium compounds with different numbers of $3d$ electrons [2]. According to them, $\Delta E = K\beta 1 - K\beta' = 8.3$ eV, and the intensity ratio $I(K\beta 1)/I(K\beta') = 0.26$ for chromium.

2.2 Satellites from Radiative Auger Transitions

Deexcitation of an atom with a vacancy in an inner shell to a state with less energy can proceed not only through a nonradiative transition accompanied by electron emissioin or a radiative process, but is also possible through a simultaneous emission of an electron and a photon. The energy of the emitted photon in this case is given by

$$\hbar\omega + E_{\rm kin}(L) = E(KLL), \tag{1}$$

where $E_{\rm kin}(L)$ is the kineticc enenrgy of the ejected L electron and $E(KLL)$ is the full Auger electron energy. KLL denotes that an L electron fills a K-vacancy and another L electron is ejected as an Auger electron.

The evidence for a KLL radiative Auger effect, RAE, was first reported by Aberg and Utriainen [3] in 1969 and proposed as an additional decay mode for single K vacancy states in atom. The spectrum observed by them is shown in Figure 1. On the lower energy side of the Kα1, Kα2 lines, some continuum and peak structures are seen.

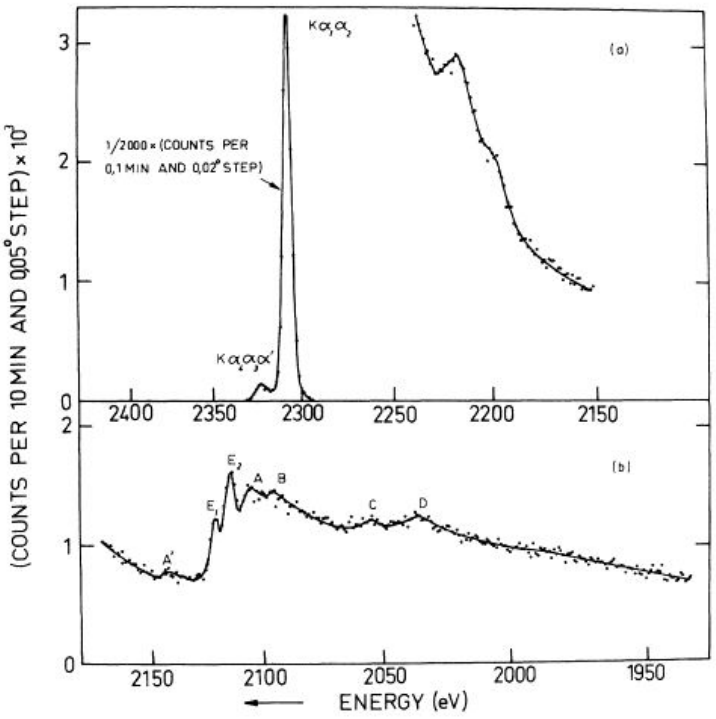

Figure 1: The lower energy side of the S Kα1, Kα2 lines [3]. (a) Two unidentified peaks. (b) The peaks identified in [3]. The spectra shown in (a) and (b) were recorded from separate samples, the counting rates being slightly different in the region of overlap.

The intensity ratio of RAE and main line and the energy of the RAE were observed by many authors [4]-[9]. The paper [9] shows many information and good summary about RAE. According to this paper, the complete processing fit of Ni X-ray spectrum becomes like Figure 2. And the detail of intensity ratio is shown in Figure 3. The intensity ratio of RAE KLL/Kα is $O(0.1)$ %, RAE KLM/Kα is $O(1)$ % and RAE KMM/Kβ is $\sim$ 2-3$\times$KLM/Kα %. The data table [6] has many calculated values of RAE energy. However some approximation must be applied to fit the RAE region, because the structure of RAE is complicated by the continuum photon energy.

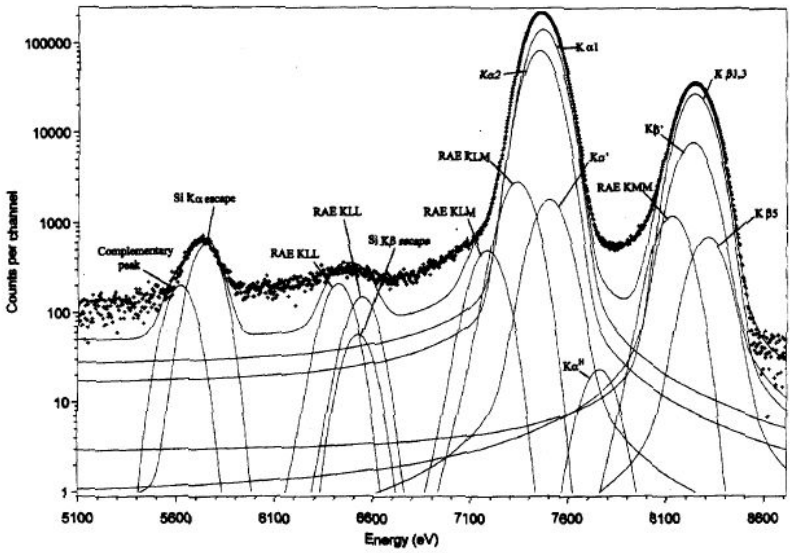

Figure 2: Complete processing of nickel fluorescence X-ray spectrum [9].

2.3 Satellites from Transitions Between Multiply Ionized States

If an additional electron is missing in any shell during a transition that leads to an X-ray emission, the energy of emitted photon is, in general, larger than the initial diagram line.

Table 1. Kβ/Kα and radiative Auger effect/main line intensity ratios

Element	22 Ti	23 V	24 Cr	25 Mn	26 Fe	27 Co	28 Ni	29 Cu
Fitting with 2 Gaussians	0.1359(17)	0.1363(17)	0.1394(17)	0.1383(17)	0.1372(17)	0.1379(17)	0.1377(17)	0.1358(17)
Complete fitting	0.1368(17)	0.1385(17)	0.1400(17)	0.1396(17)	0.1419(19)	0.1385(17)	0.1386(17)	0.1388(17)
EC decay*		0.1465(35)	0.1411(21)	0.1385(17)	0.1423(17)	0.1382(28)		0.1366(16)
RHF theory†	0.1355	0.1367	0.1337	0.1385	0.1391		0.1401	0.1379
MCDF theory‡	0.133		0.1352		0.1366		0.1365	0.1377
Evaluated values§	0.1325(18)	0.1334(16)	0.1346(14)	0.1359(14)	0.1368(14)	0.1372(14)	0.1378(14)	0.1391(14)
RAE KLL/Kα (%)	0.40(1)	0.25(1)	0.22(1)	0.22(1)	0.21(1)	0.10(1)	0.18(1)	0.10(1)
RAE KLM/ Kα (%)	1.19(5)	1.48(5)	1.21(4)	1.37(4)	1.03(3)	1.20(3)	0.80(2)	0.78(2)
RAE KMM/ Kβ (%)	2.6(2)	6.4(2)	3.2(1)	2.5(1)	3.5(4)	6.8(2)	1.7(1)	1.2(1)

The uncertainties corresponding to the standard deviation are expressed in terms of the last digit(s) and given in parentheses.
*Lépy *et al.*, 1997b.
†Scofield, 1974.
‡Jankowski and Polasik, 1989.
§Schönfeld and Janßen, 1995.

Figure 3: Kβ/Kα and radiative Auger effect/main line intensity ratios [9].

Know processes leading to multiply ionized atoms include successive ionization, multiple ionization by radiationless (Auger) transitions and multiple ionization through electron and photon collisions. Of these, only the indirect multiple ionization through Auger transitions and the direct multiple ionization (shake-off) [10] need be considered because of short lifetime of the X-ray vacancy.

But in the K series cannot be explained by indirect multiple ionization since multiply ionized states with a K-vacancy cannot be created through the Auger effect. So only direct ionization must be considered to discuss K series satellites.

The K series satellites due to direct multiple ionization were investigated by many authors [10]-[21]. Especially [15] is a unique paper for observation of the projectile Z dependence of satellites energy and intensity using Bragg spectrometer. Figure 4 shows the Titanium Kα X-ray spectra excited by fast heavy ions. But "fast" means several MeV kinetic energy for protons, not corresponding to ~ 130 MeV/c pions of our situation. Even so the fact that the 2.5 MeV protons cannot ionize double L electrons is clear from Figure 4.

The experimental Titanium KL^n X-rays centroid energies are shown in Figure 5. KL^n denotes the X-rays emitted when one K vacancy and n L vacancies exist. The centroid energies of same n increase with the projectile Z does. If n increase one, one more L vacancy exists, the difference of the energies is about 30 eV.

Percent of total Kα intensity in the diagram line and satellites vs energy per amu of

projectile is shown in Figure 6 and 7. From these figures, faster the projectile velocity is, smaller the intensity ratio $I(KL^n)/I(KL^0)$ is for $Z = 1$ projectile.

According to [13], K X-ray shifts due to a missing $2p$ electron become like Figure 8. The shifts of Kβ X-rays are about 80 eV. Figure 9 shows the energy level diagram for the removal of a $2p$ electron. The binding energy of each level is increased and the magnitude is $K > L > M$, so the Kβ X-rays shifts become larger than Kα X-rays one.

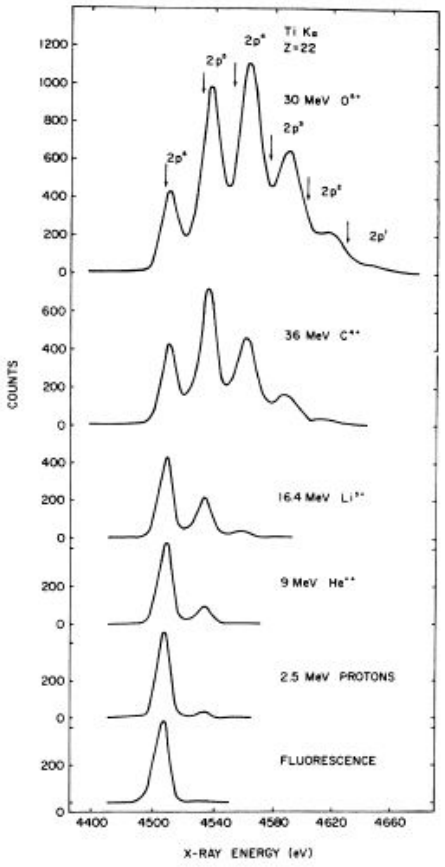

Figure 4: Titanium Kα X-ray spectra. The arrows indicate Hartree-Fock energies for these peaks assuming no vacancies in the M and N shells. [15].

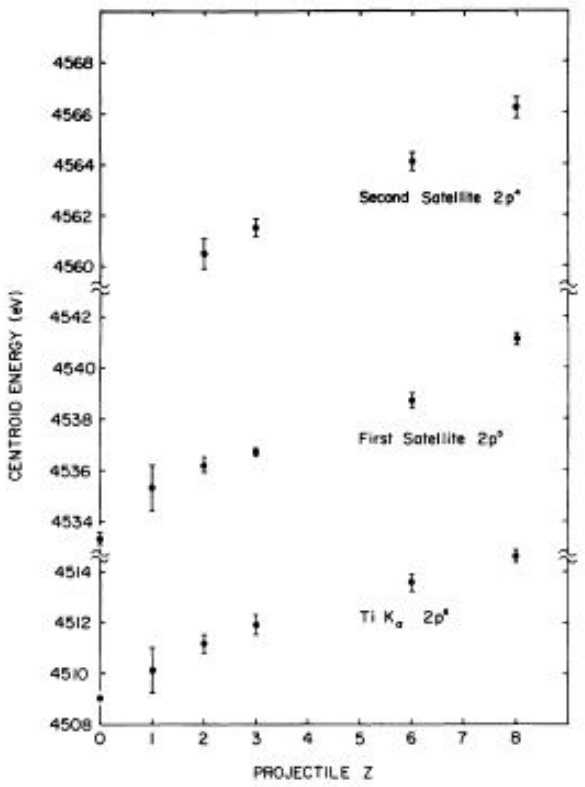

Figure 5: Experimental Ti KL^n centroid energies as a function of projectile Z for $n = 0, 1, 2$ [15].

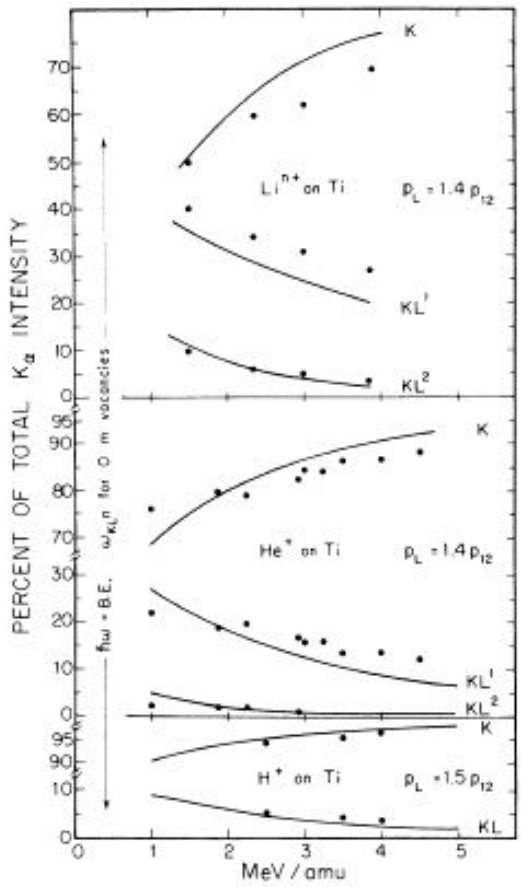

Figure 6: Percent of total Kα intensity in the diagram line and satellites vs energy per amu of projectile for H^+, Ne^{n+} and Li^{n+} [15].

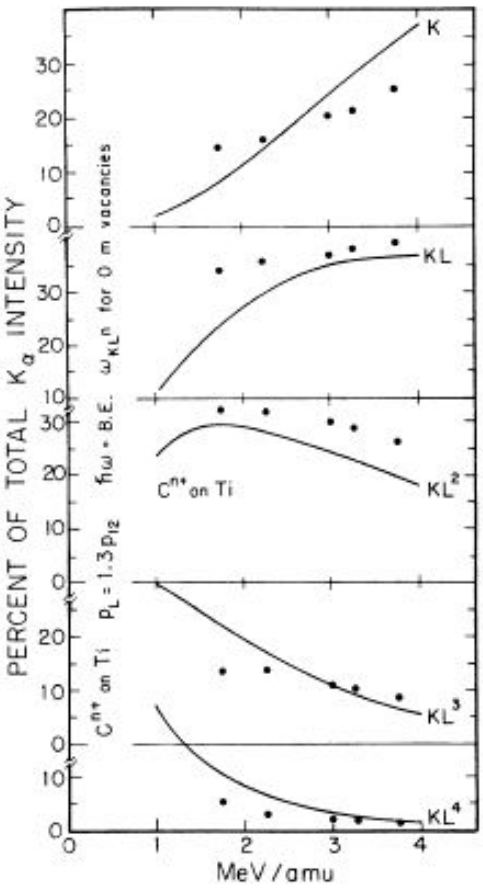

Figure 7: Percent of total Kα intensity in the diagram line and satellites vs energy per amu of projectile for C^{n+} [15].

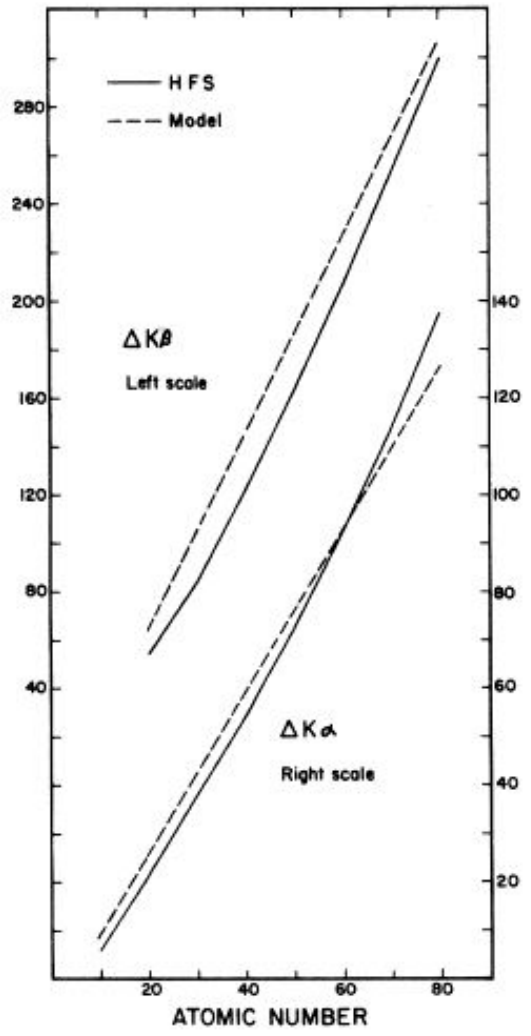

Figure 8: K X-ray energy shifts in eV due to missing $2p$ electron [13]. The HFS results (solid curves) are compared to the simple model (dashed curves).

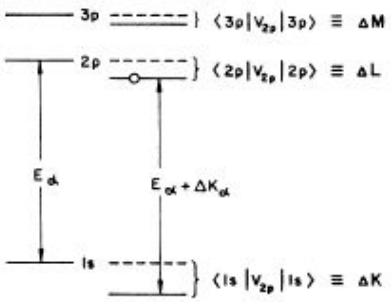

Figure 9: Binding-energy level diagram for the removal of a $2p$ electron. The binding energy of each level is increased. [13].

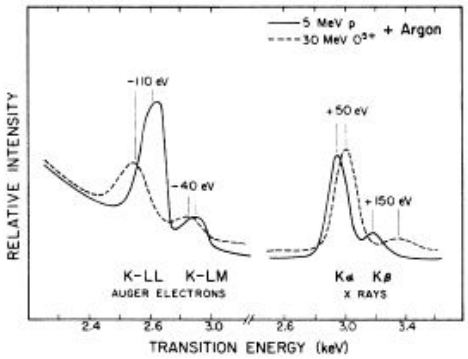

Figure 10: K X-ray and Auger electron spectra of Ar produced by 30 MeV oxygen ions (dashed curves) and 5 MeV protons (solid curves). The indicated energy shits are due to multiple ionization. [13].

3 SDD Test Experimental Data Analysis

The fit result of spill off spectrum Figure 11.

```
FCN=8847.72 FROM MINOS     STATUS=SUCCESSFUL   4848 CALLS        6444 TOTAL
EDM=0.144951    STRATEGY= 1      ERROR MATRIX ACCURATE
 EXT PARAMETER                   PARABOLIC         MINOS ERRORS
 NO.   NAME      VALUE            ERROR      NEGATIVE      POSITIVE
  1  G mean Ka1   2.01080e+03   1.88902e-02  -1.62987e-02   2.27962e-02
  2  G mean Kb1   2.20884e+03   3.78053e-02  -3.61908e-02   4.20657e-02
  3  G sigma Ka1   2.55211e+01   1.35833e-02  -1.59682e-02   1.21289e-02
  4  Fano         1.20000e-01     fixed
  5  G height Ka1   3.61994e+05   2.48965e+02  -2.72144e+02   2.43355e+02
  6  Ka1 Kb1 ratio   1.55120e+00   2.10278e-03  -2.15728e-03   2.19523e-03
  7  Escape ratio   3.11285e-03   5.93974e-05  -5.97103e-05   6.30377e-05
  8  TS height    5.87309e+03   1.48802e+02  -1.18220e+02   1.91248e+02
  9  i_{T} factor   9.54940e-01   4.21180e-04  -3.31042e-04   5.34957e-04
 10  S height     4.46658e+02   5.06243e+00  -4.76188e+00   5.57825e+00
 11  D height     2.63970e+03   8.43433e+01  -7.31318e+01   9.91222e+01
 12  D slope      1.80974e+02   5.04533e+00  -5.62411e+00   4.56498e+00
 13  TiKa1 height   5.73055e+02   1.64265e+01  -1.58464e+01   1.79998e+01
 14  ESCcomp height   7.90665e+02   2.90099e+01  -2.95130e+01   3.05440e+01

 ndf            =   110
 chi^2          =   8847.72
 chi^2/ndf      =   80.4339
 e2c            =   2.98787 +- 0.000659925 [eV/ch]
 intercept      =  -109.273 +- 1.32826     [eV]
```

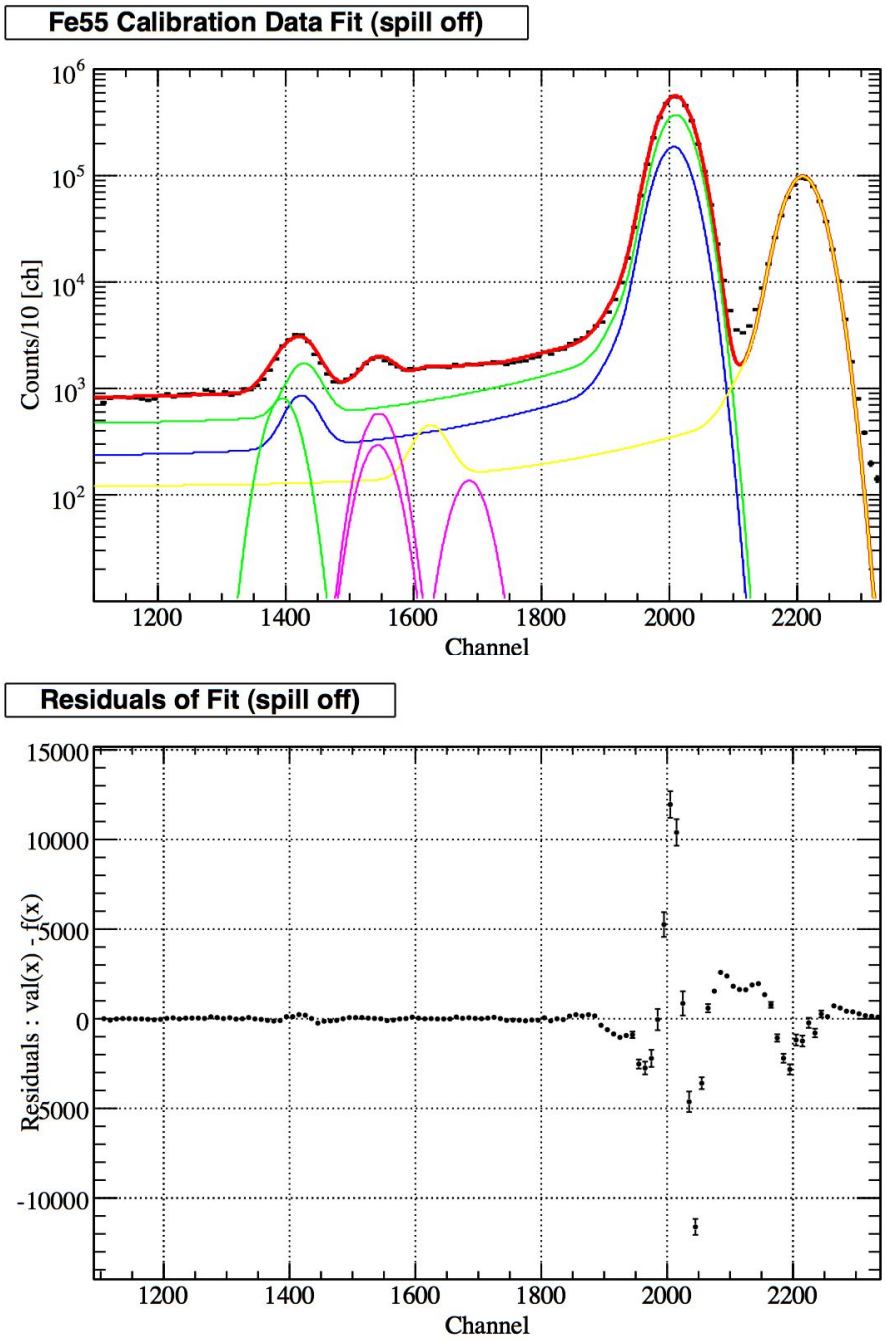
Fe55 Calibration Data Fit (spill off)
Counts/10 [ch]
Channel
Residuals of Fit (spill off)
Residuals : val(x) -f(x)
Channel

Figure 11: .

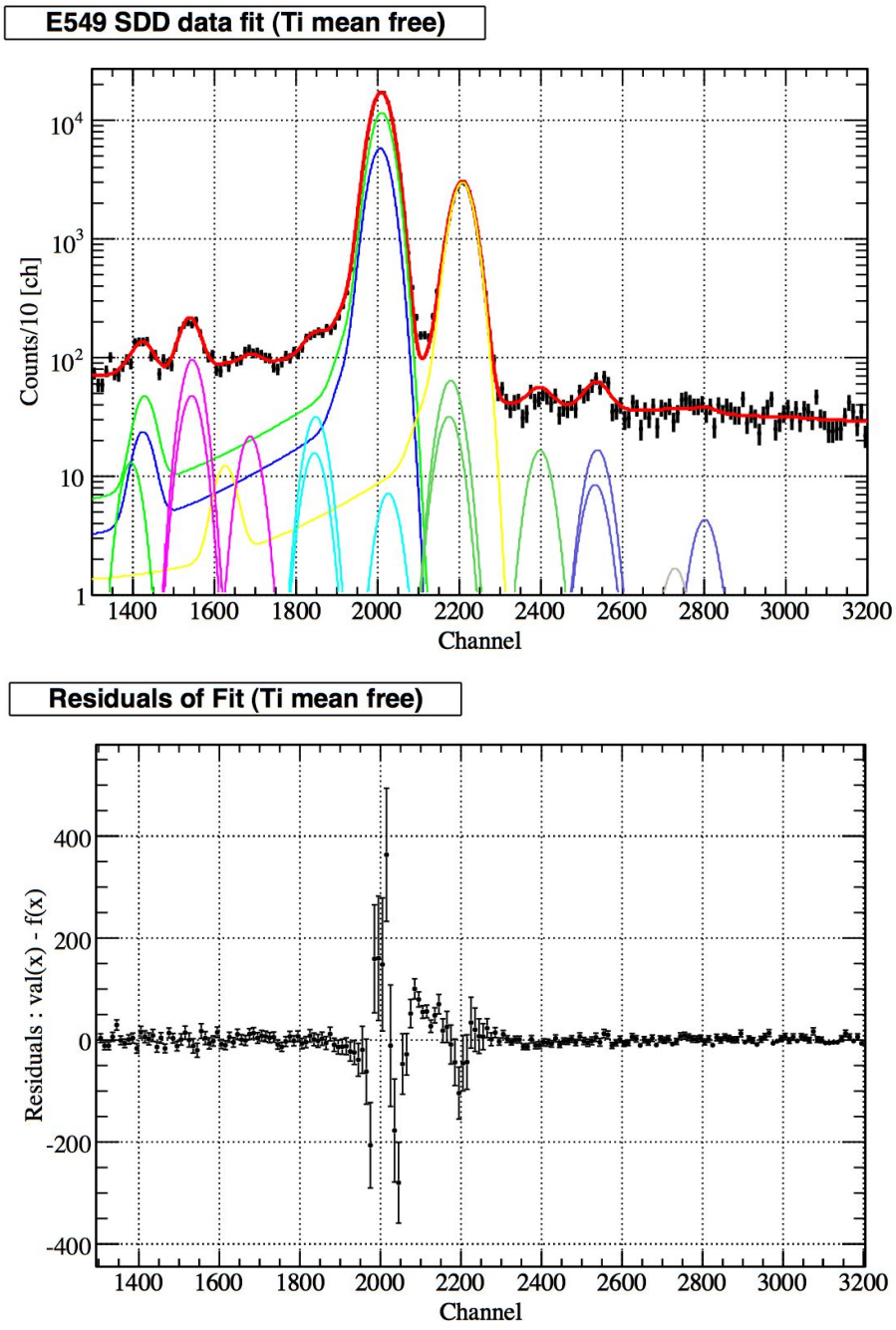
E549 SDD data fit (Ti mean free)
Counts/10 [ch]
Channel
Residuals of Fit (Ti mean free)
Residuals : val(x) - f(x)
Channel

Figure 12: .

The fit result of spill on Ti side spectrum Figure 12.

```
 FCN=333.322 FROM MINOS     STATUS=SUCCESSFUL   7045 CALLS       17290 TOTAL
 EDM=3.68986e-06    STRATEGY= 1  ERROR MATRIX UNCERTAINTY
0.3 per cent
  EXT PARAMETER                   PARABOLIC         MINOS ERRORS
  NO.   NAME      VALUE            ERROR      NEGATIVE      POSITIVE
   1  G mean Ka1   2.01068e+03   9.83471e-02  -9.81198e-02   1.00020e-01
   2  G mean Kb1   2.20849e+03   2.57878e-01  -2.59014e-01   2.59216e-01
   3  G sigma Ka1   2.56042e+01   7.26295e-02  -7.37890e-02   7.31096e-02
   4  Fano         1.20000e-01     fixed
   5  G height Ka1   1.12787e+04   4.34360e+01  -4.35000e+01   4.35200e+01
   6  Ka1 Kb1 ratio   1.51126e+00   1.50175e-02  -1.50482e-02   1.49958e-02
   7  Escape ratio   3.43219e-03   4.13131e-04  -4.25666e-04   4.25124e-04
   8  TS height    1.46429e+02   2.02609e+01  -1.95191e+01   2.18831e+01
   9  i_{T} factor   9.50909e-01   2.39705e-03  -2.42151e-03   2.43895e-03
  10  S height     4.62335e+00   1.97893e+00  -1.97403e+00   1.97559e+00
  11  D height     8.99877e+01   1.21357e+01  -1.22177e+01   1.21896e+01
  12  D slope      1.80000e+02     fixed
  13  TiKa1 height   9.40788e+01   4.97623e+00  -4.94042e+00   4.94468e+00
  14  Comp height   1.27596e+01   6.52831e+00  -6.80155e+00   6.83301e+00
  15  CrKa1 height   3.09880e+01   6.12160e+00  -6.11215e+00   6.11317e+00
  16  FeKb1 height   1.62240e+01   2.96911e+00  -2.98858e+00   2.98424e+00
  17  NiKa1 height   1.64679e+01   2.42113e+00  -2.44275e+00   2.44583e+00
  18  CuKa1 height   1.65095e+00   1.85556e+00   at limit      1.96361e+00
  19  Bg const     4.58530e+00   2.29079e-02  -2.35998e-02   2.30282e-02
  20  Bg slope    -3.85443e-04     fixed
  21  G free Ka1 mean   1.53776e+03   2.17353e+00  -2.18455e+00   2.20089e+00
  22  G free Kb1 mean   1.68926e+03   6.57793e+00  -6.61697e+00   6.55799e+00

  ndf            =   171
  chi^2          =   333.322
  chi^2/ndf      =   1.94925
  e2c            =   2.99117 +- 0.00419469 [eV/ch]
  intercept      =  -115.522 +- 8.43937    [eV]
  Ti Ka1 mean    =   4484.17 +- -6.85862   [eV]
  Ti Kb1 mean    =   4937.34 +- -19.7525   [eV]
  diff Ka1 mean  =  -26.6706 +- -6.85862   [eV]
  diff Kb1 mean  =   5.53135 +- -19.7525   [eV]
```

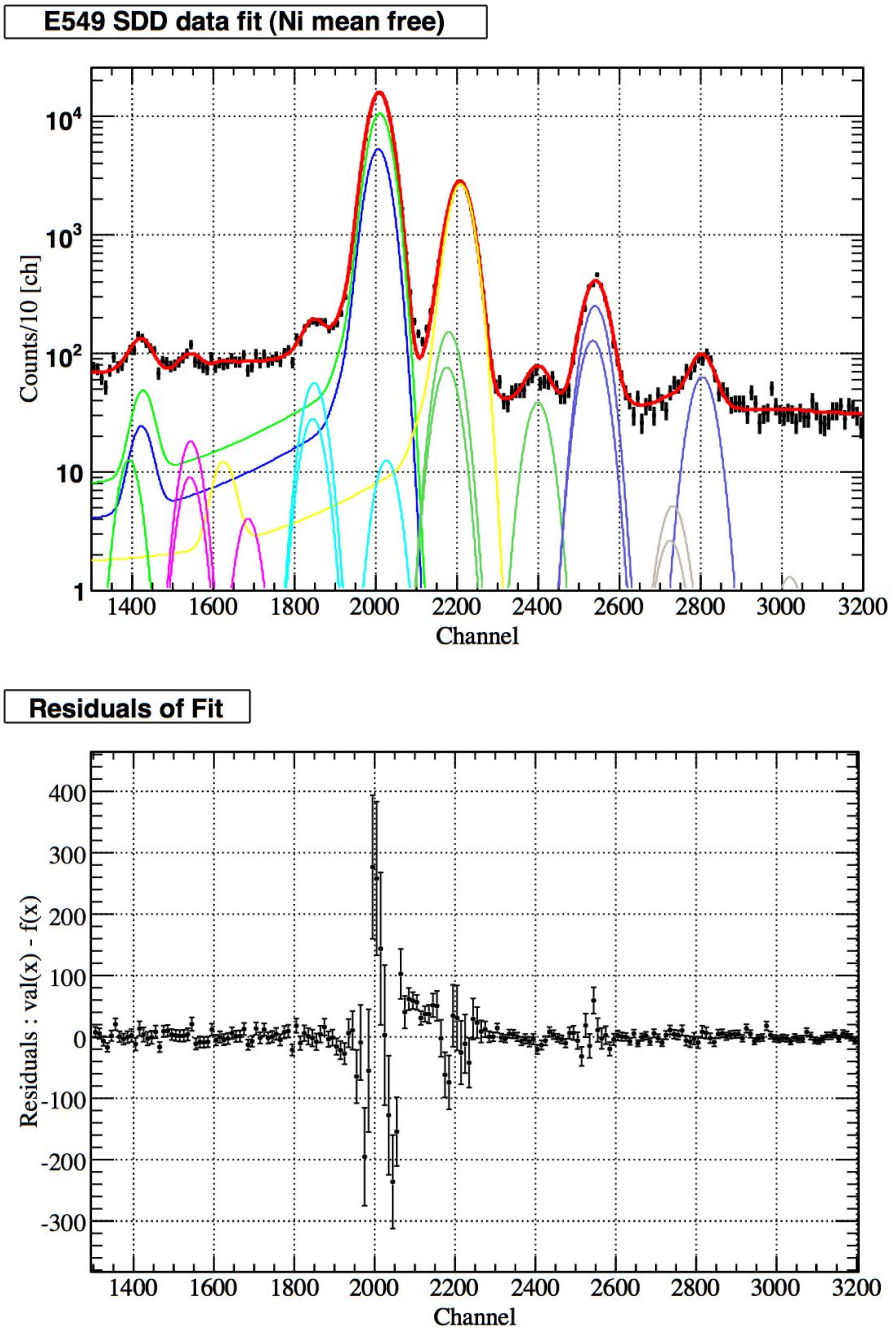
E549 SDD data fit (Ni mean free)
Counts/10 [ch]
Channel
Residuals of Fit
Residuals : val(x) - f(x)
Channel

Figure 13: .

The fit result of spill on Ni side spectrum Figure 13.

```
FCN=294.317 FROM MINOS     STATUS=SUCCESSFUL  10423 CALLS       17290 TOTAL
EDM=6.31568e-07    STRATEGY= 0  ERROR MATRIX UNCERTAINTY   1.3 per cent
 EXT PARAMETER                   PARABOLIC         MINOS ERRORS
 NO.   NAME      VALUE            ERROR      NEGATIVE      POSITIVE
  1  G mean Ka1   2.01081e+03   1.16288e-01  -1.16168e-01   1.22334e-01
  2  G mean Kb1   2.20935e+03   2.60448e-01  -2.78024e-01   2.79683e-01
  3  G sigma Ka1   2.55976e+01   7.76067e-02  -8.53481e-02   8.32913e-02
  4  Fano         1.20000e-01     fixed
  5  G height Ka1   1.02924e+04   3.96940e+01  -4.29633e+01   4.26138e+01
  6  Ka1 Kb1 ratio   1.48948e+00   1.55936e-02  -1.69986e-02   1.69314e-02
  7  Escape ratio   3.72106e-03   4.15785e-04  -4.61155e-04   4.60985e-04
  8  TS height    1.47979e+02   2.95845e+01  -2.76701e+01   3.48240e+01
  9  i_{T} factor   9.55883e-01   3.17458e-03  -3.22617e-03   3.21210e-03
 10  S height     6.47144e+00   1.82789e+00  -1.87862e+00   1.88504e+00
 11  D height     7.75891e+01   1.14400e+01  -1.17335e+01   1.16543e+01
 12  D slope      1.80000e+02     fixed
 13  TiKa1 height   1.78051e+01   3.54454e+00  -3.73990e+00   3.73770e+00
 14  Comp height   1.23298e+01   6.46017e+00  -6.67969e+00   6.69254e+00
 15  CrKa1 height   5.54055e+01   5.86380e+00  -6.24306e+00   6.23611e+00
 16  FeKb1 height   3.80359e+01   3.06854e+00  -3.17870e+00   3.16639e+00
 17  NiKa1 height   2.46815e+02   5.20187e+00  -5.31972e+00   5.32039e+00
 18  CuKa1 height   5.08012e+00   2.17297e+00  -2.37136e+00   2.36723e+00
 19  Bg const     4.40483e+00   2.09167e-02  -2.46680e-02   2.40511e-02
 20  Bg slope    -3.07978e-04     fixed
 21  G free Ka1 mean   2.54443e+03   9.64808e-01  -9.91505e-01   9.85281e-01
 22  G free Kb1 mean   2.80342e+03   2.48863e+00  -2.66456e+00   2.60081e+00

 ndf            =   171
 chi^2          =   294.317
 chi^2/ndf      =   1.72115
 e2c            =   2.98024 +- 0.00455247 [eV/ch]
 intercept      =  -93.9406 +- 9.16104    [eV]
 Ni Ka1 mean    =   7489.06 +- 3.83465    [eV]
 Ni Kb1 mean    =   8260.92 +- 8.64329    [eV]
 diff Ka1 mean  =   10.9139 +- 3.83465    [eV]
 diff Kb1 mean  =  -3.74498 +- 8.64329    [eV]
```

References

[1] K. Tsutsumi *J. Phys. Soc. Jpn.* **14** (1959) 1696

[2] K. Tsutsumi, H. Nakamori *J. Phys. Soc. Jpn.* **25** (1968) 1418

[3] T. Aberg, J. Utriainen, *Phys. Rev. Lett.* **22** (1969) 1346

[4] T. Aberg, *Phys. Rev. A* **4** (1971) 1735

[5] P. Richard *et al*, *Phys. Lett.* **54A** (1975) 169

[6] F.P. Larkins, *At. Data and Nucl. Data Tables* **20** (1977) 311

[7] M. Budnar *et al*, *Nucl. Instrum. Methods B* **63** (1992) 377

[8] J.L. Campbell *et al*, *X-ray Spectrometry* **26** (1997) 223

[9] Marie-Martine Be *et al*, *Appl. Radiat. Isot.* **49** (1998) 1367

[10] Robert D. Richtmyer, *Phys. Rev.* **49** (1936) 1

[11] Anna W. Pearsall, *Phys. Rev.* **48** (1935) 133

[12] P. Richard *et al*, *Phys. Rev. Lett.* **23** (1969) 1009

[13] D. Burch *et al*, *Phys. Rev. A* **9** (1974) 1007

[14] James H. Scofield, *Phys. Rev. A* **9** (1974) 1041

[15] K.W. Hill *et al*, *Phys. Rev. A* **13** (1976) 1334

[16] F.C. Jundt and D.J. Nagel, *Phys. Lett.* **50A** (1974) 179

[17] Y. Awaya *et al*, *Phys. Lett.* **61A** (1977) 111

[18] M.H. Chen *et al*, *Phys. Rev. A* **25** (1982) 391

[19] Moshe Deutsch, *Phys. Rev. A* **39** (1989) 1077

[20] O. Mauron *et al*, *Phys. Rev. A* **62** (2000) 062508

[21] Matjaz Kavcic, *Phys. Rev. A* **68** (2003) 022713